

# Evidence for stellar driven outflows from the Classical T Tauri Star RY Tau

Ana I. Gómez de Castro<sup>1</sup> and Eva Verdugo<sup>2</sup>

<sup>1</sup> Instituto de Astronomía y Geodesia (CSIC-UCM)  
Facultad de CC. Matemáticas, Univ. Complutense  
Madrid, E28040 Spain

<sup>2</sup> European Space Astronomy Centre (ESAC)  
Research & Scientific Support Dept.- ESA  
P.O.Box 50727, Madrid, E28080 Spain

## ABSTRACT

RY Tau is a rapidly rotating Classical T Tauri star observed close to edge-on. The combination of new HST/STIS observations obtained in 2001 with HST/GHRS Archive data from 1993 has allowed us to get, for the first time, information on the thermal structure and the velocity law of the wind. The repeated observations of the Si III] and C III] lines show a lack of changes with time in the blue side of the profile (dominated by the wind contribution). Very high temperature plasma ( $\log T_e = 4.8$ ) is detected at densities of  $9.5 \leq \log n_e(\text{cm}^{-3}) \leq 10.2$  associated with the wind. The emitting volumes are  $\sim (0.35R_\odot)^3$  suggesting a stellar origin. The wind kinematics derived from the profiles (Si III] , C III] and [O II] ) does not satisfy the theoretical predictions of MHD centrifugally driven disk winds. The profiles' asymmetry, large velocity dispersions and small variability as well as the small emitting volumes are best explained if the wind is produced by the contribution of several outflows from atmospheric open field structures as those observed in the Sun.

**Keywords:** stars: pre-main sequence — stars: winds,outflows — stars : individual(RY Tau)

# 1 Introduction

Winds from T Tauri Stars (TTSs) were assumed to be cold, in spite of the observational evidence of our own Sun, because they were first detected as bipolar molecular outflows (Loren et al 1981) and optical jets with low ionization fractions. The detection of C III] and Si III] semiforbidden line emission from RY Tau and RU Lup wind (Gómez de Castro & Verdugo, 2001; hereafter GdCV) provided the first evidence that electron temperatures as high as  $\log Te(K) \simeq 4.5$  could be achieved at the base of the TTSs outflows; this high temperature was derived from ultraviolet (UV) observations and could not be inferred from the classical optical/infrared/radio tracers. Recently, Dupree et al (2005) have claimed that O VI absorption has been detected in TW Hya and T Tau. These new data represent a challenge to the current theories for outflow generation in TTSs. In this letter, we provide observational evidence of hot winds being driven from the stellar atmosphere of RY Tau, a rapidly rotating TTS ( $v \sin i = 51.6$  km/s, Hartmann & Stauffer, 1989). RY Tau has been classified as an UX Ori star: a pre-main sequence star which shows aperiodic eclipse-like minima caused by variable obscuration produced by circumstellar dust associated with the disk (Grinin, 1992). This suggests that the disk is seen close to edge-on. Also, the high projected rotation velocity of the stellar atmosphere suggests that the star inclination is close to  $90^\circ$ .

# 2 Data

Some few spectral tracers have been selected for the subsequent study, namely, the C IV , C III] , [C II] , Si III] and [O II] lines observed in the UV spectrum of RY Tau (see Table 1 for more details on the observations and the line fluxes, and Fig. 1 for the profiles). All data are public and can be withdrawn from the HST Archive (they were obtained either by us or by other HST users). Data have been processed with the Routine Science Data Pipeline (RSDP). The major source of inaccuracy in the calibration is the centering of the target in the aperture that can account for as much as  $20 \text{ km s}^{-1}$  in the wavelength zeropoint accuracy of the GHRS data (see GdCV) and  $<0.1\text{-}0.2$  pixels in the STIS data (*e.g.* velocity zeropoint accuracies better than  $0.6 \text{ km s}^{-1}$  and  $2.8 \text{ km s}^{-1}$  for the E230M and G230M spectra, respectively). WAVECALs were obtained during the observations and the pickup procedure (ACQ/PEAK) was used for the acquisition to center the source accurately, to about a 5% of the slit width (see [www.stsci.edu/hst/stis/](http://www.stsci.edu/hst/stis/) for more details). This accuracy was cross-checked for the E230M spectra using as reference the narrow absorption features observed in the Fe II, Mg II and Mg I resonance lines produced by the interstellar medium. The STIS spectra were co-added after this check to improve the SNR of the data since no variations are detected. The profiles have been classified in Fig 1 by observing date. The left panel displays the very asymmetric C III] and Si III] profiles that led GdCV to conclude that these lines are produced at the base of the wind. The C IV line observed  $\sim 2$  hours before is also displayed; the

profile is very similar to the C III] and Si III] lines. Bluewards shifted emission is also detected in the [O II] lines (see central panel) observed in Feb. 2001. The [C II] , Mg II and Mg I lines are obtained in the same spectra. A minimum is detected at a similar velocity in the Mg II lines; these lines have large optical depths in dense plasmas with  $T \simeq 10^4\text{K}$ . A narrow absorption component, probably of interstellar origin, is detected at the stellar rest velocity. There also seems to be an absorption component in the Mg I line at the same velocity. The last observations of the C III] and Si III] lines are displayed in the right panel of Fig.1. The profiles changed significantly from 1993 to 2001, although the bluewards shifted part of the profile remains stable.

### 3 Interpretation and Analysis

The detection of emission from high velocity gas in C IV , Si III] , C III] , [O II] , [O I] (Hamann 1994) indicates that *there is a broad range of temperatures in the RY Tau wind at similar velocities*. The wind properties seem to be rather stable; *the emission peaks at similar bluewards shifted velocities in observations obtained over 10 years*, compare Fig. 1 with Hamann (1994) that measures a blueshifted [O I] emission peaking at -79 km/s.

Line ratios can be used to constrain the wind temperature and density taking into account that the regions traced by each spectral tracer only overlap partially. Also occultation effects may be relevant (see Sect.4). Line emissivities have been calculated for a collisional plasma over a broad range of densities ( $n_e = 10^7 - 10^{13} \text{ cm}^{-3}$ ) and temperatures ( $\log T_e(K) = 4.0 - 5.0$ ) using the atomic parameters in the CHIANTI data base (Dere et al 1997) and assuming solar abundances and ionization equilibrium.

*The high temperature region:* from the GHRS observations we derive: C IV /Si III] =  $0.6 \pm 0.7$  and Si III] /C III] =  $1.1 \pm 0.6$ . Then from Fig. 2 we derive:  $\log(T_e) \simeq 4.8$  and  $9.5 < \log(n_e) < 10.2$ . *Neither the line ratios nor the UV line fluxes vary by more than a factor of 2 in the fifteen observations available from 1979 to 2001 (GdCV)*. Notice that the high resolution data indicate that the variable contribution from 0-velocity and redshifted material to the Si III] and C III] line fluxes does not significantly change their line ratios <sup>1</sup>.

*The low temperature region:* The [C II] emission feature consists of five spectral lines (see Fig. 1 and Table 1). The individual features are not resolved in RY Tau; a broad blend is observed instead. Some ratios among the individual lines in the feature are *density sensitive* in the range  $n_e = 10^8 - 10^{11} \text{ cm}^{-3}$ . An accurate determination of the electron density in the [C II] emission region requires us to derive simultaneously the ratios among the multiplet lines and the underlying [C II] profile. A least

---

<sup>1</sup>  $\left[ \frac{\text{Si III]}}{\text{C III]}} \right]_{\text{GHRS}} = 1.1 \pm 0.6$ ,  $\left[ \frac{\text{Si III]}}{\text{C III]}} \right]_{\text{STIS}} = 1.7 \pm 0.5$ ,  $\left[ \frac{\text{Si III]}_{\text{STIS}} - \text{Si III]}_{\text{GHRS}}}{\text{C III]}_{\text{STIS}} - \text{C III]}_{\text{GHRS}}} \right] = 4 \pm 3$  Thus the average physical conditions of this hot plasma in the wind are similar to those derived from the redshifted material.

squares scheme has been used to solve this inverse problem. The optimal fit gives a high lower limit of  $n_e > 10^{10} \text{ cm}^{-3}$  for the [C II] emitting region, similar to that determined from the C III] line. Note that the [C II] profile is too noisy to narrow this range (the contribution from the Fe II(uv3) line at vacuum wavelength 2328.11Å is negligible as shown by the weakness of nearby features corresponding to the same multiplet). The fit also indicates that the underlying [C II] profile is similar to the C III] (STIS) profile; *e.g.* a blueshifted wind profile plus an excess from 0-velocity to the redwards shifted edge. From that fit, we also obtain  $\frac{F(C \text{ II})_{2326.117}}{F(C \text{ III})_{1908.7}} = 1.3 \pm 0.1$ . This ratio is *temperature sensitive* and from that we derive that  $4.4 < \log(T_e) < 4.5$ .

## 4 Implications for wind models

TTSs outflows are characterized by their collimation at large scales, *i.e.*, it is expected that whatever the ejection mechanism is, the wind terminal speed corresponds to a longitudinal motion along the collimation axis. Current models make use of magnetic fields to guarantee the large scale collimation. In this section we use the models of Gómez de Castro & Ferro-Fontán 2005 (hereafter GdCFF) to compare to data. Disk wind models by other authors have a similar kinematics though the scales are different (see Uzdensky 2004 for a review).

In GdCFF models, the wind is launched from the disk corona by a combination of thermal pressure and centrifugal force. This results in a radial expansion, away from the rotation axis, at the base and produces an increasing broadening of the profiles in this acceleration region. After this, the restoring toroidal component of the field narrows down the beam and the velocity field is progressively dominated by the motion along the rotation axis until it reaches the asymptotic regime, *i.e.* flow along the axis at the terminal velocity and basically no radial expansion. The evolution of the radial expansion,  $V_r$ , with the height above the disk is plotted in the top panel of Fig 3 for the warm disk winds model. Line emission is produced at different locations in the flow depending on densities and temperatures thus, the line profiles depend on the region of the wind sampled by each particular spectral indicator (as well as on the inclination).

In order to compare these theoretical predictions with the observations, we have defined two observables that are measured only from the bluewards shifted emission of the relevant spectral tracers to avoid the pollution by the contribution of the accretion flow. Notice that line emission from high temperature infalling plasma is produced at scales  $\ll R_*$  pumped by the X-ray radiation released at the accretion shocks. Thus occultation by the stellar disk causes the contribution to the line flux from accretion to be redwards shifted (see Beristain et al (2001) for more details). These observables are the velocity dispersion,  $dV$ , and the line centroid,  $V_c$ . The line profiles may be understood as velocity-flux plots (or  $V - f$  plots). The centroid of the bluewards shifted region of the profile is defined as,  $V_c = \frac{\sum_{i=1}^N f_i (V_0 + i\Delta V)}{\sum_{i=1}^N f_i}$  and the

dispersion,  $dV$ , as,  $dV = \sqrt{\frac{\sum_{i=1}^N f_i ((V_0 + i\Delta V)^2 - V_c^2)}{\sum_{i=1}^N f_i}}$  for a uniformly sampled profile with step  $\Delta V$  and  $N$  points.  $V_0$  represents the velocity at the blue edge of the profile and  $N = ABS(V_0/\Delta V) + 1$ . These observables have been calculated for three spectral tracers that sample very different plasma densities: Si III] , C III] and [O II] . The critical electron densities for the collisional quenching of the C III] and [O II] lines are  $1.5 \times 10^{10} \text{ cm}^{-3}$  and  $0.5 \times 10^7 \text{ cm}^{-3}$  respectively. For comparison, the critical density of the Si III] line is  $2.0 \times 10^{12} \text{ cm}^{-3}$  for a fiducial temperature of  $2.5 \times 10^4 \text{ K}$ .  $V_c$  and  $dV$  are plotted in the bottom panel of Fig 3 for the GdCFF theoretical predictions and various inclinations; notice that the [O II] line is predicted to be formed in the rarified expanding region while the C III] and Si III] lines are predicted to be formed in the hot disk corona where the wind is accelerated.

$V_c$  and  $dV$  have been computed for the [O II] , C III] and Si III] profiles observed in RY Tau. To take into account the effect of the noise on these observables, we have computed these values both on the observed profiles and on filtered profiles obtained by applying a white noise filter to the data. As shown in Fig. 3, the major effect of the noise is to increase the velocity dispersion and shift the centroid some few  $\text{km s}^{-1}$  to the blue; however the overall trend remains. Two important results are derived from the figure:

1. The line centroid shifts to higher velocity as the density traced by the spectral line becomes lower as expected (see critical densities),
2. The velocity dispersion is high,  $> 40 \text{ km s}^{-1}$ , and similar for all the tracers. In addition, the profiles are very asymmetric (see Fig. 1). Rather constant velocity dispersions and asymmetric profiles are expected for very small inclinations, while for large inclinations the profiles should be symmetric and the dispersion increase steadily with the line centroid. However, all evidence points to RY Tau being observed close to edge-on (see Sect. 1).

Thus RY Tau observations cannot be reconciled with models based on the centrifugal launching of the TTSs jets from the accretion disk.

Another important piece of evidence comes from the emitting volumes. The volume of plasma producing the observed Si III] and C III] flux can be derived from the line emissivity<sup>2</sup>. The emitting volume producing the Si III] emission is  $2.07 \times 10^{31} \text{ cm}^3$  (*i.e.*  $(0.24 R_\odot)^3$ ) and similar to the derived for the C III] and C IV lines. Thus, line emission is produced in either a small structure or in dense clumps in the outflow. Notice that even adopting a filling factor of 0.1%–1% for the clumps, as that derived from observations of optical jets (Liseau et al 1996), the volume of the region producing the observed C III] and Si III] profiles just increases to about  $1.1 - 2.4 R_\odot$ . Thus, it is highly likely that mass ejection occurs from the stellar surface.

---

<sup>2</sup>The emissivities are:  $j(\text{C IV}) = 1.44 \times 10^{-2} \text{ erg cm}^{-3} \text{ s}^{-1}$  for  $\log(T_e) = 4.8$  and  $\log(n_e) = 11$ ;  $j(\text{Si III])} = 1.49 \times 10^{-2} \text{ erg cm}^{-3} \text{ s}^{-1}$  for  $\log(T_e) = 4.8$  and  $\log(n_e) = 11$ ; and  $j(\text{C III])} = 0.97 \times 10^{-3} \text{ erg cm}^{-3} \text{ s}^{-1}$  for  $\log(T_e) = 4.8$  and  $\log(n_e) = 11$ .

As RY Tau is a fast rotator the centrifugal lever arm from the stellar surface is an efficient source of thrust (see *e.g.* Sakurai 1987). Thus, the wind could be ejected from the stellar surface from open field structures like those observed in the Solar corona. The interaction between the wind and the circumstellar material (and a probable slow wind) could produce shocked knots like the Corotating Interaction Regions (CIRs) observed in the interplanetary medium and in young stars like AB Dor (Gómez de Castro 2002) that could contribute to the UX Ori phenomenon observed in RY Tau.

This suggestive possibility would indicate that the observed profiles represent just an average of many small scale outflows and although these would not be stationary on a one-by-one basis, the average of all of them could produce a rather stable profile (provided that the spectral resolution is not good enough to resolve the individual components). If the magnetic field configuration is not axisymmetric (as observed in cool main sequence stars) this wind would naturally lead to the formation of nonaxisymmetric outflows. Tracking the variability of the C IV and C III] profiles is crucial for testing this possibility.

**Acknowledgments:** We thank an anonymous referee for helping us to sharpen the definition of the observables in Fig. 3.

## References

- [1] Ardila, D. R., Basri, G., Walter, F. M., Valenti, J. A., Johns-Krull, C. M., 2002, ApJ, 566, 1100
- [2] Beristain, G. Edwards, S., Kwan, J., 2001, ApJ, 551, 1037
- [3] Dere, K. P., Landi, E., Mason, H. E., Monsignori Fossi, B. C., Young, P. R., 1997, A&AS, 125, 149
- [4] Dupréé, A. K., Brickhouse, N. S., Smith, Graeme H., Strader, Jay, 2005, ApJ, 626, L59
- [5] Gómez de Castro, A.I., Verdugo, E., 2001, ApJ, 548, 976
- [6] Gómez de Castro, A.I., 2002, MNRAS, 332, 409
- [7] Gómez de Castro, A.I., Ferro-Fontán, C., 2005, MNRAS, 365, 569
- [8] Grinin, V.P., 1992, A&AT, 3, 17
- [9] Hamman, F., 1994, ApJS, 93, 485
- [10] Hartmann, L., Stauffer, J.R., 1989, AJ, 97, 873
- [11] Liseau, R., Hultgren, M., Fridlund, C.V.M., Cameron, M., A&A, 306, 255

- [12] Sakurai, T., 1985, A& A, 152, 121
- [13] Uzdensky, D., 2004, Ap&SS, 292, 573

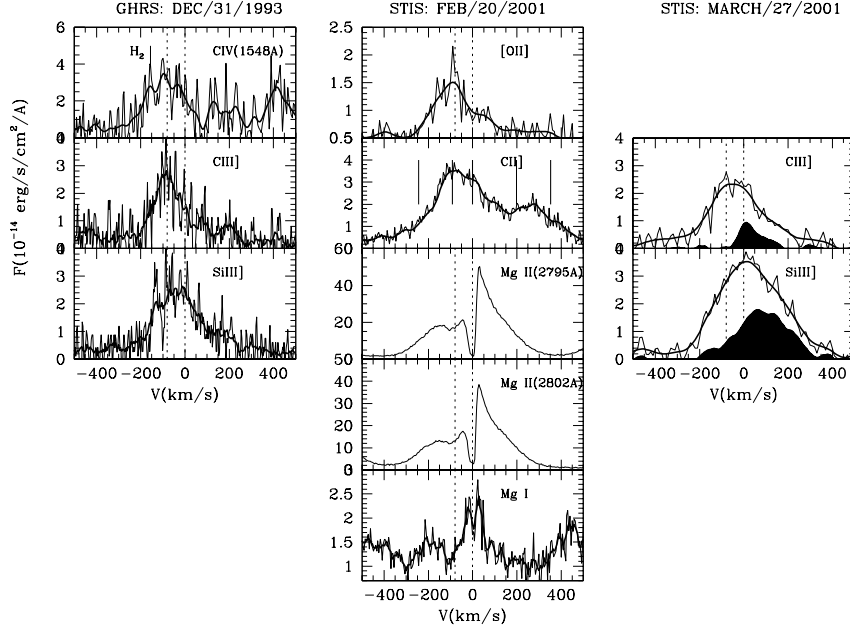


Figure 1: UV lines observed in RY Tau and used in this work; RSDP processed data (see Table 1 for the binning) are plotted with a thin line and the 3-pixels average profile with a thick line. The rest wavelength of the lines and the velocity of the unresolved jet at  $\simeq -80$  km/s (from GdCV and Hamann 1994) are marked with dashed lines. *Left panel:* Observations obtained in Dec. 31st, 1993 with the GHRS. The C IV line is blended with a very weak H<sub>2</sub> feature (see Ardila et al 2002). *Central panel:* Profiles from STIS observations obtained in Feb. 20-21, 2001. The 5 components of the [C II] multiplet are marked. *Right panel:* C III] and Si III] lines observed in March 27th, 2001. Both lines show an excess of flux in the red wing compared with the 1993 observations; this excess is shaded in the figure.

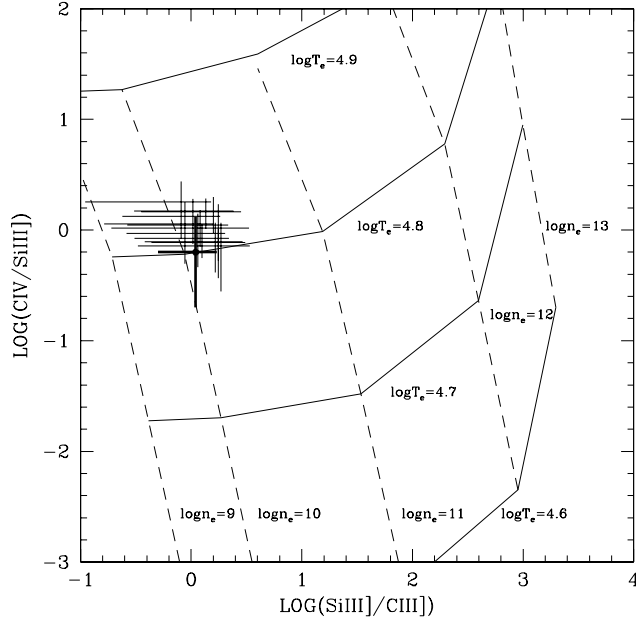


Figure 2:  $\text{C IV} / \text{Si III}]$  versus  $\text{Si III}] / \text{C III}]$  flux ratios (in  $\text{erg/s/cm}^{-2}$ ) for collisional plasmas with electron densities between  $10^9 - 10^{13} \text{cm}^{-3}$ , temperatures  $\log(T_e)=4-5$  and solar abundances. The value (with the error bars) derived from high resolution observations is marked with thick line; the 13 low resolution IUE observations are plotted with thin lines. Isothermal and isochoric lines are plotted with continuous and dashed lines respectively.

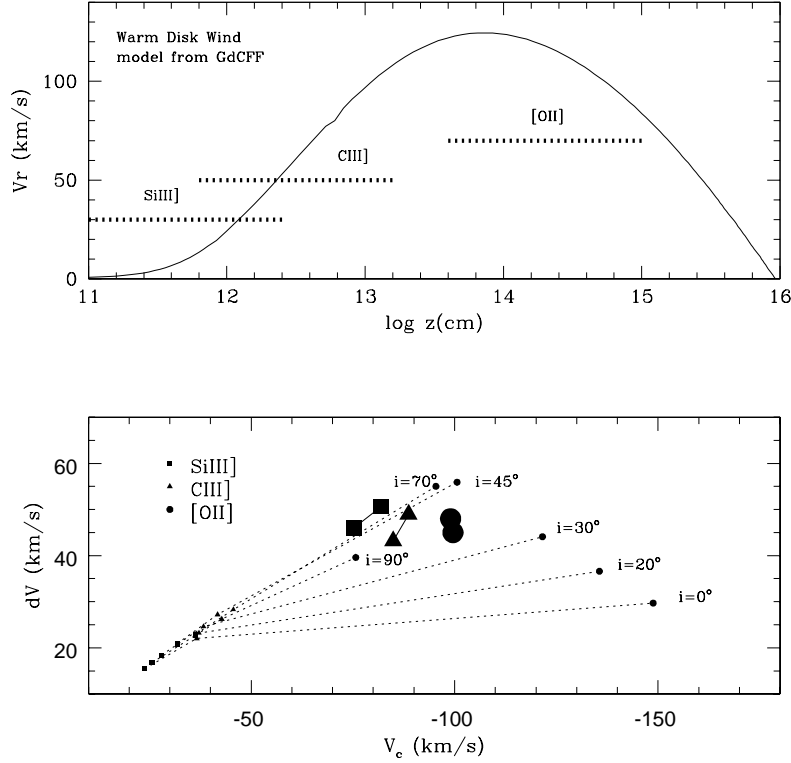


Figure 3: *Top*: variation of the wind expansion velocity with respect to the jet axis,  $V_r$ , with the height above the disk,  $z$ , from GdCFF model. The location of the [Si III], [C III] and [O II] emission regions is sketched (see GdCFF for the detailed calculations). *Bottom*: Comparison between the theoretical predictions from the GdCFF model and RY Tau observations.  $V_c$  and  $dV$  values measured from the [Si III], [C III] and [O II] profiles observed in RY Tau are marked with big squares, triangles and circles respectively.  $V_c$  and  $dV$  are plotted from the [Si III], [C III] and [O II] profiles derived from the theory (small symbols) for various inclinations. High  $dV$  values are obtained from the observed profile while the slightly smaller  $dV$  values are measured over filtered profiles (see text).

Table 1: HST/STIS observations.

Inst.	Grating	Res.	Scale <sup>(a)</sup>	Slit	Spec. Range	Obs. Date	Target <sup>(b)</sup> Features	Flux <sup>(c)</sup>
			Å/elem		Å	(dd-mm-yyyy)		10 <sup>-14</sup> (erg/s/cm <sup>2</sup> )
GHRS <sup>(d)</sup>	G160M	20000	0.069	LSA <sup>(e)</sup>	1532 - 1567	31-12-1993	C IV	F(C IV)= 8.2 ± 7.1 <sup>(g)</sup>
	G200M	20000	0.078	LSA	1880 - 1920	31-12-1993	Si III], C III] F(C III)] = 12 ± 3	F(Si III)] = 13 ± 4
STIS <sup>(g)</sup>	E230M	30000	1/60,000	0".2x0".2	2303 - 3111	19-02-2001	[O II], [C II], Mg II, Mg I	F([O II]) = 5.5 ± 1.4
	E230M	30000	1/60,000	0".2x0".2	2303 - 3111	20-02-2001	[O II], [C II], Mg II, Mg I	F([C II] <sub>2326.1</sub> ) = 19 ± 2
	E230M	30000	1/60,000	0".2x0".2	2303 - 3111	20-02-2001	[O II], [C II], Mg II, Mg I	
	G230M	10500	0.09	52"x0".2	1839 - 1929	27-03-2001	Si III], C III]	F(Si III)] = 26 ± 3 F(C III)] = 15 ± 3

<sup>(a)</sup> The element is a diode for GHRS spectra and a pixel for STIS spectra.

<sup>(b)</sup> The vacuum wavelengths of the target features are: C IV(1548Å, 1550Å), Si III](1892Å), C III](1908Å), [O II] (2471Å), [C II](2324.2Å, 2325.4Å, 2326.1Å, 2327.6Å, 2328.8Å), Mg II (2796Å, 2803Å), Mg I (2853Å)

<sup>(c)</sup> The Interstellar reddening law has been used since the extinction law towards T Tauri systems is not known.  
Parameters:  $A_V=0.55\text{mag}$ ;  $A_{CIV}/A_V = 2.60$ ;  $A_{SiIII}/A_V = 2.66$ ;  $A_{CIII}/A_V = 2.66$ ;  $A_{CII}/A_V = 2.60$ ;  $A_{OII}/A_V = 2.44$ .  
The flux of the [C II](2326.1Å) has been derived from the fitting of the [C II] multiplet (see text).

<sup>(d)</sup> Goddard High Resolution Spectrograph removed in February 1997

<sup>(e)</sup> Large Science Aperture (2")

<sup>(f)</sup> The H<sub>2</sub> (3-8 R(3)) line contribution to the C IV flux is negligible (see Ardila et al 2002).

<sup>(g)</sup> Space Telescope Imaging Spectrograph stopped science operations in August 2004